

## Heat and Mass Transfer Characteristics of Alkali Metals in a Combined Wick of High-Temperature Heat Pipe

Ping Yu<sup>1,\*</sup>, Chuanhui Huang<sup>1</sup>, Lei Liu<sup>1</sup>, Huafeng Guo<sup>1</sup> and Chengqiang Liu<sup>1</sup>

**Abstract:** To study the heat and mass transfer characteristics of alkali metals in a combined porous wick in high-temperature heat pipes, a three-dimensional (3-D) numerical model is constructed by using the finite volume method, Darcy's theory, and the theory of local thermal equilibrium. The research finds that the pressure drop of fluids flowing through a combined porous wick exhibits an increasing trend with increasing flow velocity at the inlet and with decreasing permeability of the porous media; a combined porous wick of lower porosity and permeability and larger fluid velocity at the inlet is found to have a less uniformly distributed fluid velocity; the different temperatures of the fluid at the inlet mainly influence the inlet section of the computational model, while having negligible effect thereon in the axial direction (this embodies the thermal homogeneity of such heat pipes). The result reveals that the temperature change in fluids at the inlet does not significantly affect the overall temperature distribution in a combined wick.

**Keywords:** Porous medium, heat pipe, numerical simulation, combined wick.

### Nomenclature

$K_i$	the permeability of the porous media, [m <sup>2</sup> ]
$P$	pressure, [Pa]
$T$	temperature, [K]
$q$	heat flux, [W/m <sup>2</sup> ]
$\bar{U}$	velocity vector, [m/s]
$u$	velocity scalar, [m/s]
$h$	the total energy, [J]
$k$	thermal conductivity, [W/(m·K)]
$H_{\text{vap}}$	the latent heat of vaporisation, [kJ/kg]

<sup>1</sup> College of Mechanical and Electrical Engineering, Xuzhou University of Technology, Xuzhou, China.

\* Corresponding Author: Ping Yu. Email: yuping050201@163.com.

Received: 08 March 2019; Accepted: 10 June 2019.

$S_i$	the momentum source term
$C_{fi}$	the coefficient of inertial resistance

*Greek symbols*

$\varepsilon$	the porosity of the porous media
$\sigma$	the standard deviation
$\mu$	dynamic viscosity, [kg/(m·s)]
$\rho$	density, [kg/m <sup>3</sup> ]

*Subscript*

l	fluid
g	solid matrix of the porous media
eff	effective
i	$i=x, y, z$ , representing three mutually orthogonal coordinate direction

**1 Introduction**

High-temperature heat pipes, using alkali metals as the working fluid, are characterised by advantages, such as favourable thermal homogeneity, high operational efficiency, and an excellent safety record [Zhuang and Zhang (2000); Yu, Zhang, Xu et al. (2015)], so they are widely used in a variety of high-temperature conditions, including thermal protection of flanges of aircraft [Liu and Liu (2016); Wang, Qu and Huai (2015)], receivers of disk solar thermal power generation [Shen, Zhang, Xu et al. (2015)], and in nuclear reactors [Wang, Guo, Zhang et al. (2013)]. The wick in a heat pipe provides cyclic power for working media and thereby determines the axial heat transfer capacity of the heat pipe, so the structure of the wick and the heat and mass transfer mechanism therein have become a focus for researchers in various disciplines. Bai [Bai (2011)] developed a combined wick for high-temperature heat pipes, which mainly comprises two parts: the metal fibre felt for producing capillary suction and the triangular groove functioning as the circulation channel. This type of wick is able to guarantee the advantages of large capillary suction and small flow resistance at the same time. With such advantages, it can enhance the heat transfer capacity of high-temperature heat pipes, and also ensures the safe operation thereof, thus avoiding the occurrence of dry-out. Yu et al. [Yu, Zhang, Xu et al. (2014, 2015)] studied the solid-liquid transition process of working media in the porous wick of high-temperature heat pipes with alkali metal as the working fluid in the initiating stage. In the simulation process, the influences of non-Darcian effects and the natural convection of liquid alkali metals were taken into consideration. In this way, they found that the melting rate of alkali metals is related to the porosity and permeability of the porous wick. Besides, they also studied the flow characteristics of the liquid alkali metals in the porous wick. Han et al. [Han, Chai, Zhou et al. (2014)] established a solid-liquid-gas three-phase coupling mathematical model using the simulation software to investigate the heat and mass transfer mechanisms of high-temperature heat pipes taking potassium as the working fluid. The simulation results matched experimental data. The analysis of the simulation results reveals the heat and mass transfer mechanisms in the high-temperature heat

pipes with potassium as the working fluid, and provides theoretical support for such experiments and the optimisation of heat pipe designs. Wu et al. [Wu, Cao, Xiao et al. (2012)] built a constant-temperature phase-transition model for capillary wicks based on alkali-metal thermoelectric converters to analyse the influences of parameters including the thickness and porosity of wicks, as well as the flow velocity and temperature of working media, on the velocity, and temperature, fields in capillary wicks. Moreover, they also explored the relationship between the maximum capillary suction and the pressure drop around the loop and proposed a range of values for the effective pore size and suggested measures with which to improve the performance of porous wicks. Shen et al. [Shen, Zhang, Xu et al. (2016)] studied the heat transfer performance of alkali metal heat pipes experimentally. They found that thermal conductivity of wick has the greater impact, while thicknesses of wick has the smaller impact on heat transfer performance of alkali metal heat pipe.

A high-temperature heat pipe with an alkali metal as the working fluid is composed of an evaporator section, a condenser section, and an adiabatic section. The heat pipe does not allow heat transfer between the internal and external parts in the adiabatic section, in which the wick is used to transport the circulating working media. If the working media cannot be transported from the condenser section to the evaporator section timeously, there will be no adequate working media in the evaporator section to absorb heat, such that the heat pipes must fill to work properly and will even suffer burn-down. This makes it a necessity to study the heat and mass transfer characteristics of working media in the wick in the adiabatic section; however, there is little research available on this topic, therefore, the current research involved construction of a physical model for the adiabatic section of a high-temperature heat pipe with sodium as the working medium and a combined wick and established a mathematical model based on the finite volume method, Darcy's theory, and local thermal equilibrium theory. In addition, the term of momentum loss source for the combined porous wick was considered in the momentum balance equation. On this basis, the pressure drops along the working media flow through the combined wick in the adiabatic section of the high-temperature heat pipe, and the velocity, and temperature, fields were investigated.

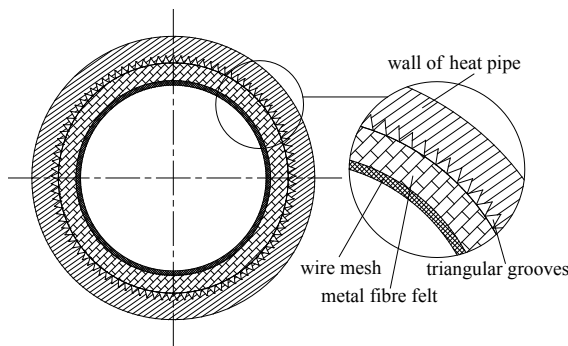
## 2 Mathematical and physical models

### 2.1 Physical model

The 400-mm-long high-temperature heat pipe had an outer diameter of 32 mm, in which the evaporator section, the adiabatic section, and the condenser section were 240, 40, and 120 mm long, respectively. The combined wick [Bai, Zhang, Xu et al. (2011)] was composed of triangular grooves, metal fibre felt, and wire mesh. The 110 triangular grooves were 0.8 mm wide and 0.8 mm deep (Fig. 1). The metal fibre felt was soft and its different thicknesses resulted in distinct porosities of the combined wick. The metal fibre felt of three different thicknesses and the triangular grooves were combined to prepare wicks of three different porosities and permeabilities (numbered: #1, #2, and #3). Salient test parameters are listed in Tab. 1 and details of the preparation process can be found elsewhere [Bai (2011)].

**Table 1:** Parameters of the combined wick samples

No.	The combined porous wick	
	Porosity/%	Permeability/ $10^{-10} \text{ m}^2$
#1	96.9	3.37
#2	96.4	2.46
#3	96.0	1.05

**Figure 1:** Physical model

## 2.2 Mathematical model

The mathematical model was constructed according to the size of the combined wick. The following assumptions were made for the model: the flow was stable; the acceleration due to gravity was ignored (i.e., self-weight effects were deemed negligible); both the fluid and the combined porous wick had constant physical properties; the fluid flowed in the porous media and the additional loss of momentum was added to the momentum equation; the porous media and the fluid were governed by local thermal equilibrium; and porous media were isotropic, homogeneous, and filled with fluid.

The following equation is obtained according to the above model and assumptions:

The loss of momentum in the porous media comprises both viscous and inertial loss terms, and is expressed as:

$$S_i = -\left(\frac{\mu u_i}{K_i} + \frac{C_{fi}}{2}\rho_l u_i^2\right) \quad (1)$$

Continuity equation

$$\nabla \cdot (\rho_l \bar{U}) = 0 \quad (2)$$

Momentum equation

$$\nabla \cdot (\rho_l \bar{U} u_i) = \nabla \cdot (\mu \cdot \nabla u_i) - \frac{\partial p}{\partial x_i} + S_i \quad (3)$$

Energy conservation equation

$$\frac{\partial}{\partial t}[\varepsilon\rho_1h_1 + (1-\varepsilon)\rho_g h_g] + \nabla \cdot (\bar{U}\rho_1h_1) = \nabla \cdot (k_{\text{eff}} \nabla T) \quad (4)$$

where,  $\mu$ ,  $u_i$ ,  $K_i$ ,  $C_{fi}$ ,  $\rho_1$ ,  $\rho_g$ ,  $\bar{U}$ ,  $p$ , and  $S_i$  refer to the dynamic viscosity of the fluid, the velocity scalar of the fluid ( $i=x, y, z$ , representing three mutually orthogonal coordinate direction), the permeability of the porous media, the coefficient of inertial resistance of the fluid, the density of the fluid, the density of the solid matrix of the porous media, the velocity vector, the pressure, and the momentum source term, respectively. Meanwhile,  $\varepsilon$ ,  $h_1$ ,  $h_g$ ,  $T$ , and  $k_{\text{eff}}$  represent the porosity of the porous media, the enthalpy of the fluid, the enthalpy of the solid matrix of the porous media, the temperature, and the effective thermal conductivity ( $k_{\text{eff}} = \varepsilon k_1 + (1-\varepsilon)k_g$ , where  $k_1$  and  $k_g$  are the thermal conductivities of the fluid and the solid matrix of the porous media, respectively). In accordance with Darcy's law, the viscous loss term in the momentum source term  $S_i$  is directly proportional to the fluid velocity and the coefficient of inertial resistance  $C_{fi}$  is zero, if the fluid flow in the porous media is laminar. According to the Darcy-Forchheimer law [Beavers and Sparrow (1969); Jiang, Chen, Jin et al. (2015); Zhong, Liu, Tao et al. (2011)], the momentum source term contains that additional part resulting from consideration of inertial resistance effects when the fluid flow in the porous media is turbulent. With reference to the literature [Bai (2011)] the coefficient of inertial resistance  $C_{fi}$  is calculated as:

$$C_{fi} = \frac{a}{1 + e^{(-b*(Re - c))}} \quad (5)$$

where,  $Re$  represents the Reynolds number of fluid flow in the metal fibre felt.

$$a = 135.9e^{\frac{\delta}{5.19 \times 10^{-4}}} + 16176.1 \quad (6)$$

$$b = 2043.8\delta - 2.1 \quad (7)$$

$$c = 7.3 - 2536.1\delta + 282130\delta^2 \quad (8)$$

where,  $\delta$  refers to the thickness of the metal fibre felt. The state of the fluid flow, laminar or turbulent, is determined according to the Reynolds number:

$$Re = \frac{ud_w\rho_1}{\mu} \quad (9)$$

For fibrous material, the characteristic size,  $d_w$ , is the diameter of the fiber. The metal fibre felt (Bekipor® WB 08/300) is provided by Bekipor Company from Belgium, where 08 represents the fiber diameter of  $8 \mu\text{m}$ . When  $Re < 1$ , the fluid flow in the metal fibre felt is a laminar state, and  $Re > 1$  for a turbulent state.

### 2.3 Numerical model

The fluid region of the combined wick includes the following parts: region 1-the triangular grooves and region 2-the annulus formed by the metal fibre felt (Fig. 2). As the model is symmetrical, to reduce the amount of computation required, only the combined wick formed by one triangular groove and the corresponding metal fibre felt

is taken as the research object (Fig. 3).

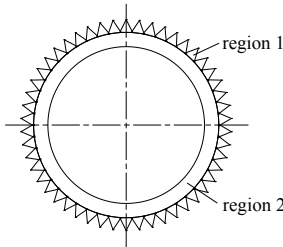


**Figure 2:** Cross-section of the combined wick

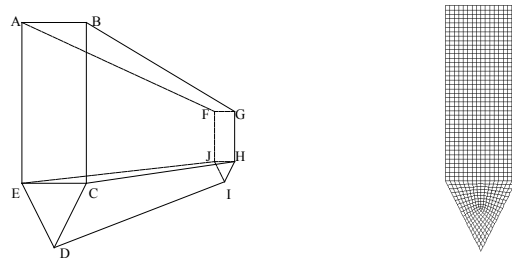


**Figure 3:** Calculation model

**Figure 4:** Local grid

The unstructured tetrahedral mesh and the hexahedral structural mesh are used when constructing the regions of the triangular groove and metal fibre felt, respectively. The model comprises 691,200 elements, 2,127,264 faces, and 745,731 nodes (Fig. 4). The velocity-inlet and outflow boundary conditions are applied to the inlet (face  $S_{ABCDE}$ ) and the outlet (face  $S_{FGHIJ}$ ) of the numerical model, separately. As the research focuses on the adiabatic section of the high-temperature heat pipe, the face  $S_{ABGF}$  connected to the steam chamber is at the saturation temperature of liquid sodium (1,154.55 K), and the two side faces ( $S_{BCHG}$  and  $S_{AFJE}$ ) are set to be symmetrical. The overlapped interface ( $S_{ECHJ}$ ) between the two fluid regions of the triangular groove and the metal fibre felt is set as an internal interface and the others are adiabatic faces. The volume control technique is applied to disperse the equation using the second-order upwind scheme. The velocity and pressure are coupled by adopting the SIMPLE algorithm. The model is calculated at steady condition. The density, the specific heat capacity, heat conductivity coefficient and the viscosity of the liquid sodium is 760.4 kg/m<sup>3</sup>, 1268 J/(kg·K), 52.6 W/(m·K), and  $1.62 \times 10^{-4}$  kg/(m·s), respectively.

### 3 Results and discussion

#### 3.1 Model verification

To validate the correctness of the model, the distribution of internal surface temperature  $T_{Ri}$  of the porous wick was numerically simulated at a flow velocity of 0.002 kg/s of the liquid sodium in accordance with previous research [Wu, Cao, Xiao et al. (2012)]. In the process, the selection of physical parameters, boundary conditions, and dimensions were chosen with reference to the literature [Wu, Cao, Xiao et al. (2012)].  $L_w$  refers to

the axial length of the porous core in the literature [Wu, Cao, Xiao et al. (2012)]. The simulated results in the current research were compared with those published elsewhere [Wu, Cao, Xiao et al. (2012)], and it was found that the maximum relative error was only 0.08% (Fig. 5): the numerical model was thus verified as being correct.

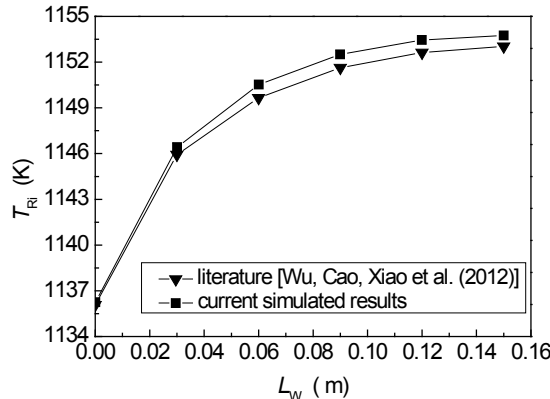


Figure 5: Comparison between current research and literature

### 3.2 Relationship between the flow velocity of liquid sodium at the inlet and the pressure drop

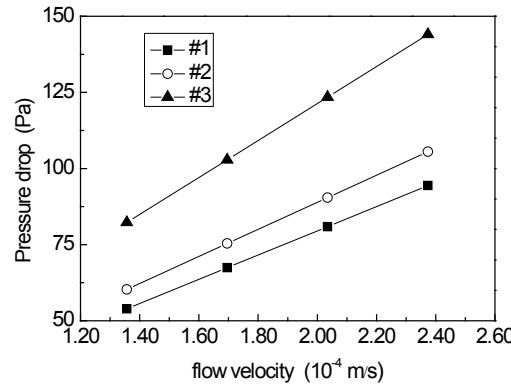
The input heat flux in the evaporator section of the high-temperature heat pipe with sodium as the working media and the combined wick is in the range of 40 to 70 W/cm<sup>2</sup> [Bai (2011)], and the circulation velocity of liquid sodium in the combined wick can be calculated using the following formula:

$$u = \frac{q}{H_{vap}\rho} \quad (10)$$

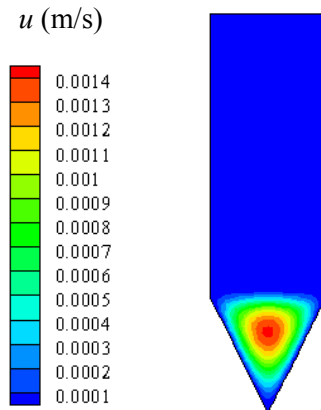
where  $q$  represents the heat flux in the evaporator section and  $H_{vap}$  refers to the latent heat of vaporisation. The flow velocity of liquid sodium at the inlet of the computational model is calculated to be between  $1.36 \times 10^{-4}$  and  $2.37 \times 10^{-4}$  m/s. According to Eq. (9), the fluid flow in the combined wick is in the laminar state within the range of this velocity.

Fig. 6 illustrates the change of the pressure drop of the liquid sodium after flowing through the combined wick with the flow velocity at the inlet: the two parameters have a linear relationship, and the pressure drop increases with increasing flow velocity of liquid sodium at the inlet. For the porous media of combined wicks #1, #2, and #3, the pressure drop across the liquid sodium increases by 26.98, 30.16, and 41.16 Pa after flowing through the combined wicks with the increase in the flow velocity of the liquid sodium at the inlet changes from  $1.70 \times 10^{-4}$  to  $2.37 \times 10^{-4}$  m/s. This indicates that the faster the flow velocity at the inlet, the greater the flow resistance in the combined wicks and thereby the greater the pressure drop. On the condition that the flow velocity of liquid sodium at the inlet is  $2.07 \times 10^{-4}$  m/s, the pressure drop across the liquid after flowing through the No. #1, #2, and #3 combined wicks are 80.90, 90.44, and 123.44 Pa,

respectively. This suggests that, when the liquid flows at the same velocity at the inlet, it is subjected to a greater pressure drop and meets a greater flow resistance while flowing in combined wicks with smaller porosity and permeability.



**Figure 6:** Relationship between the flow velocity and the pressure drop



**Figure 7:** Velocity distribution on the cross section of combined porous wick #1

Fig. 7 illustrates the velocity distribution of the liquid sodium on the cross section of the outlet of combined porous wick #1 under the condition that the flow velocity of the liquid at the inlet is  $1.36 \times 10^{-4}$  m/s: most of the liquid sodium flows through the channel formed by the triangular grooves in the case that the liquid sodium flows at the same velocity at the inlet. Therefore, the flow velocity of liquid sodium in the triangular grooves exceeds that in the metal fibre felt. This is mainly because the porous wick in the high-temperature heat pipe cannot provide sufficient capillary suction to allow the working liquid to flow from the condenser section to the evaporator section, unless they have a small enough effective pore size. While in turn, the smaller the effective pore size of the porous wick, the greater the flow resistance experienced by the fluid therein. Hence, to obtain a wick with a large capillary suction and small flow resistance of fluid, the combined wick is adopted, in which the metal fibre felt is mainly used to provide capillary suction while the triangular grooves form the main circulation channel for the liquid. The simulation results

agree well with the design objective of the combined wick.

### 3.3 Relationship between the fluid velocity at the inlet and the uniformity of velocity distribution of the fluid

The standard deviation  $\sigma_v$  of the velocity scalar of the fluid at the outlet of the combined wick is calculated by using the Bessel equation [Xing and Huang (2007)] to characterise the uniformity of velocity distribution of the fluid in the combined wick.

$$\sigma_v = \sqrt{\frac{\sum_{j=1}^n (u_j - \bar{u})^2}{n-1}} \quad (11)$$

where  $u_j$  denotes the velocity of the fluid at each node ( $j=1, 2, 3, \dots, n$ ) and  $\bar{u}$  represents the average velocity.

The uniformity of velocity distribution of the fluid will be influenced by the mesh quantity, so the grid independence tests is provided. For example, the inlet velocity is  $1.36 \times 10^{-4}$  m/s in the combined wick (numbered: #1)

**Table 2:** Grid independence tests

No.	Elements	Faces	Nodes	$\sigma_v$ / (m/s)
1	392196	1222532	438184	0.0002161
2	691200	2127264	745731	0.0002099
3	1340000	4123340	1443404	0.0002098

According to Tab. 2, compared with No. 2 method, the standard deviation of the outlet velocity with No. 3 changes by 0.05%, which is very small. Meanwhile considering the calculation time, so the No. 2 method is selected.

It can be seen from Fig. 8 that, with increasing flow velocity of the liquid sodium at the inlet, the standard deviation  $\sigma_v$  of the velocity scalar at the outlet of the combined wick also increases linearly. As the flow velocity of liquid sodium at the inlet is increased from  $1.36 \times 10^{-4}$  to  $2.37 \times 10^{-4}$  m/s, the standard deviation  $\sigma_v$  of the velocity scalar at the outlet of combined wicks 1, 2, and 3 increases by  $1.59 \times 10^{-4}$ ,  $1.61 \times 10^{-4}$ , and  $1.64 \times 10^{-4}$  m/s, respectively. The above analysis implies that the larger the flow velocity of the liquid sodium at the inlet, the more non-uniform the fluid velocity distribution in the combined wicks. If the liquid sodium flows at the same velocity at the inlet, the velocity of fluid in a combined wick of lower porosity and permeability exhibits a less uniform distribution.

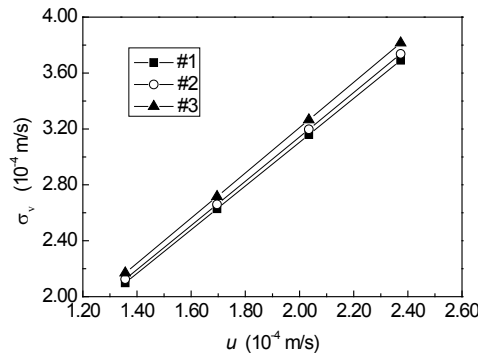


**Figure 8:** Relationship between the flow velocity and the standard deviation

### 3.4 Relationship between the fluid velocity at the inlet and the uniformity of temperature distribution in the combined wick

Fig. 9 shows the standard deviation  $\sigma_T$  of the temperature distribution on the cross-section of the combined wick along the  $z$ -axis direction when the flow velocity of the liquid sodium at the inlet is  $1.36 \times 10^{-4} \text{ m/s}$ . Fig. 10 shows the temperature distribution on the axial section of the combined wick passing the deepest point of the triangular groove in the wick. As the research focuses on the adiabatic section of the high-temperature heat pipe, the face connected to the steam chamber is at the saturation temperature of liquid sodium (1,154.55 K), so the temperature distribution is asymmetrical in Fig. 10. As shown in Figs. 9 and 10,  $\sigma_T$  decreases along the direction from the inlet to the outlet, indicating that the temperature of the combined wick becomes more uniformly distributed as the flow approaches the outlet and it finally tends to a stable value; moreover, combined wicks #1, #2, and #3 exhibit a similar trend in  $\sigma_T$ , which suggests that the combined porous wicks of different porosities and permeabilities have similar uniformity of temperature distribution.

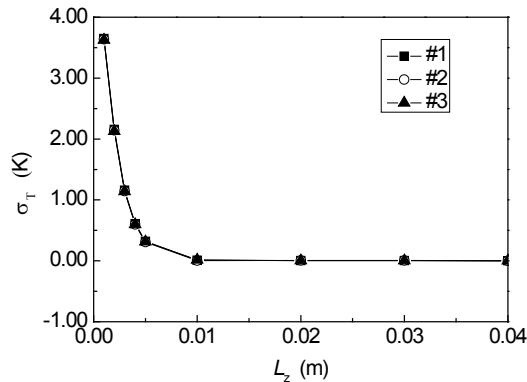


**Figure 9:** The standard deviation of the temperature distribution

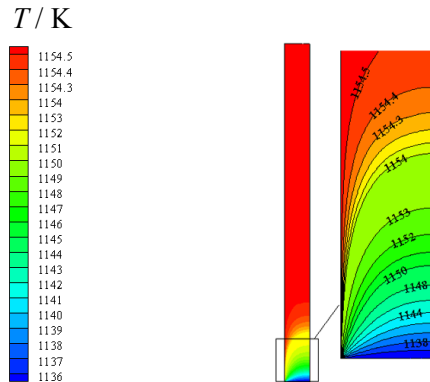


**Figure 10:** The temperature distribution on the axial section of the combined wick

### 3.5 Relationship between the flow velocity of fluid at the inlet and the cross-section temperature of the combined wicks

Fig. 11 illustrates the changes in average temperature of the cross-section of the combined wicks along the axial direction on the condition that liquid sodium flows at different velocities at the inlet, and  $v_1=1.36\times 10^{-4}$  m/s,  $v_2=2.03\times 10^{-4}$  m/s, and  $v_3=2.37\times 10^{-4}$  m/s. It can be seen from the figure that the average temperature of the cross-section of the combined wicks increases along the axial direction from the inlet and finally tends to a stable value. For combined wicks of the same porosity, the slower the flow of liquid sodium at the inlet, the higher the temperature of the cross-section of the combined wicks. Taking combined wick #1 as an example, for the cross-section at  $z=0.0064$  m, the average temperatures at that cross-section are 1,154.31 K and 1,154.29 K when the flow velocities at the inlet are  $v_1$  and  $v_3$ , respectively. The two temperatures show a difference less than 0.01%, so the difference can be ignored. Under the condition of different porosities with the same flow velocity of fluid at the inlet, the combined wicks of smaller porosity and permeability have lower average temperatures at that cross-section. For instance, if liquid sodium flows at  $v_1$  at the inlet, it is found that the average temperatures of the cross section at  $z=0.0064$  m in combined wicks #1, #2, and #3 are 1154.31, 1154.27, and 1154.25 K, separately. As the difference between the three is less than 0.01%, this was deemed negligible.

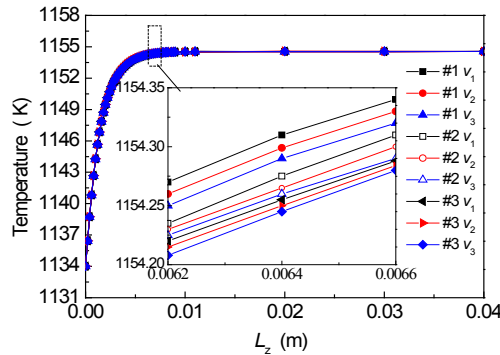


**Figure 11:** The average temperature at different flow velocities at the inlet

### 3.6 Relationship between the fluid temperature at the inlet and the cross-section temperature of the combined wicks

Fig. 12 shows the changes in average temperature of the cross-section of combined wick #1 along the axial direction with different fluid temperatures at the inlet: the different inlet temperature of the liquid sodium mainly affects the inlet section while exerts little influence in, and along, the axial direction. This reflects the thermal homogeneity of the heat pipe, therefore, changing the inlet temperature imposes insignificant effects on the overall temperature of the heat pipe.

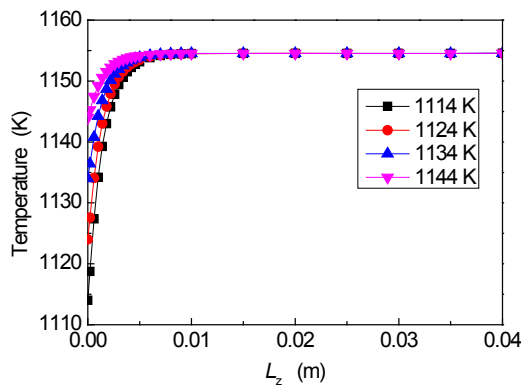


**Figure 12:** The average temperature of the cross-section of combined wick #1

## 4 Conclusions

A 3-D numerical model of a combined porous wick in the adiabatic section of the high-temperature heat pipe with sodium as the working media was established. Meanwhile, the influences of relevant parameters on the heat and mass transfer characteristics were analysed by using the finite volume method, Darcy's theory, and the theory of local thermal equilibrium. The following conclusions are obtained:

- 1) The flow velocity of liquid sodium at the inlet has a linear relationship with the pressure drop across the fluid after flowing through the combined wick. The pressure drop increases with the flow velocity of the fluid at the inlet. Besides, when the fluid flows at the same velocity at the inlet, it experiences a larger pressure drop and faces greater flow resistance after flowing through a combined wick of lower porosity and permeability.
- 2) As the flow velocity of liquid sodium at the inlet increases, the standard deviation of the velocity scalar at the outlet of the combined wick also increases linearly, which indicates that the larger the flow velocity at the inlet, the less uniform the fluid velocity distribution in the combined wick. Furthermore, if the liquid sodium flows at the same velocity at the inlet, its velocity is distributed less uniformly in a combined wick of lower porosity and permeability.
- 3) The standard deviation of the temperature distribution on a cross-section decreases along the axial direction of the combined wick. This implies that the temperature is distributed more uniformly in the combined wick while approaching the outlet and finally tends to a stable value. Moreover, the temperature of combined porous wicks of

- different porosities and permeabilities is found to be distributed with similar uniformity.
- 4) The flow velocity of liquid sodium at the inlet and the porosity and permeability of the combined wicks exert slight influences on the average cross-section temperature, so the influences thereof can be ignored. The average cross-section temperature increases along the axial direction and finally tends to a stable value.
- 5) The different inlet temperature of the liquid sodium mainly influences the inlet section while it does not significantly affect the axial direction, which evinces the thermal homogeneity of the heat pipe, therefore, changing the inlet temperature of the liquid sodium has only a slight influence on the overall temperature distribution in the computational model.

**Acknowledgement:** The present work is supported by the Natural Science Foundation of Jiangsu Province, China (Grant No. BK20180177), the Science and Technology Foundation of Xuzhou, China (Grant No. KH17007) and the Natural Science Foundation for Colleges and Universities of Jiangsu Province, China (Grant No. 17KJB460015, No. 18KJB460028).

**Conflicts of Interest:** The authors declare that they have no conflicts of interest to report regarding the present study.

## Reference

- Bai, T.** (2011): *Development and Research on Heat Transfer Performance of Combined Wick*. pp. 33-62. Nanjing Tech University. School of Mechanical and Power Engineer. China.
- Bai, T.; Zhang, H.; Xu, H.; Ding, L.** (2011): Performance study on a novel combined wick of heat pipe. *Proceedings of the CSEE*, vol. 31, no. 23, pp. 79-85.
- Beavers, G. S.; Sparrow, E. M.** (1969): Non-Darcy flow through fibrous porous media. *ASME Journal of Applied Mechanics*, vol. 36, no. 4, pp. 711-714.
- Han, Y.; Chai, B. H.; Zhou, W.; Wei, G. R.; Bi, K. M. et al.** (2014): Numerical simulation of potassium heat pipe based on porous medium model. *Atomic Energy Science and Technology*, vol. 48, no. 1, pp. 49-53.
- Jiang, H. L.; Chen, M.; Jin, Y.; Zhou, Y.; Lu, Y. H.** (2015): Analysis of plastic zone radius for open hole wellbore when a high pressure gas flows into a well. *Chinese Journal of Rock Mechanics and Engineering*, vol. 34, no. 2, pp. 4286-4294.
- Liu, H. P.; Liu, W. Q.** (2016): Effective thermal analysis of platelet heat-pipe-cooled leading edge of vehicle. *Journal of National University of Defense Technology*, vol. 38, no. 2, pp. 19-24.
- Shen, Y.; Zhang, H.; Xu, H.; Yu, P.** (2016): Simulation and experimental analysis on heat transfer characteristics of alkali metal heat pipe. *ACTA Energiae Solaris Sinica*, vol. 37, no. 3, pp. 644-650.
- Shen, Y.; Zhang, H.; Xu, H.; Yu, P.; Bai, T.** (2015): Thermal resistances of high temperature heat pipe with combined wick. *Journal of Basic Science and Engineering*, vol. 23, no. 3, pp. 541-553.

- Wang, C. L.; Guo, Z. P; Zhang, D. L.; Qiu, S. Z.; Tian, W. X. et al** (2013): Transient behavior of the sodium-potassium alloy heat pipe in passive residual heat removal system of molten salt reactor. *Progress in Nuclear Energy*, vol. 68, pp. 142-152.
- Wang, H. G.; Qu, W.; Huai, X. L.** (2015): Thermal protection of leading edge of hyper-sonic wings based on cavity heat pipes. *Journal of Engineering Thermophysics*, vol. 36, no. 10, pp. 2267-2270.
- Wu, S. Y.; Cao, B. X.; Xiao, L.; Li, Y. R.** (2012): Investigation on flow and heat transfer characteristics in capillary porous wick based on alkali metal thermal-to-electric converter (AMTEC). *Journal of Chongqing University*, vol. 35, no. 4, pp. 77-82.
- Xing, G. J.; Huang, S. Y.** (2007): *Thermal Experimental Principle and Technology*. pp. 6-8. Metallurgy Industry Press, China.
- Yu, P.; Zhang, H.; Xu, H.; Shen, Y.** (2014): Numerical simulation for solid-liquid phase change of metal sodium in combined wick. *Journal of Southeast University (English Edition)*, vol. 30, no. 4, pp. 456-461.
- Yu, P.; Zhang, H.; Xu, H.; Shen, Y.** (2015): Restart characteristics of high-temperature sodium heat pipe. *Proceedings of the CSEE*, vol. 35, no. 2, pp. 404-410.
- Yu, P.; Zhang, H.; Xu, H.; Shen, Y.; Bai, T.** (2015): Simulation for liquid sodium flow characteristics through combined wick. *Journal of Central South University (Science and Technology)*, vol. 46, no. 2, pp. 715-722.
- Zhong, W.; Liu, H.; Tao, G. L.** (2011): Theoretical and experimental investigation of flow rate characteristics of sintered metal porous media. *Journal of Mechanical Engineering*, vol. 47, no. 16, pp. 187-198.
- Zhuang, J.; Zhang, H.** (2000): *Heat Pipe Technology and Engineering Application*. pp. 5-6. Beijing: Chemical Industry Press.